Progress In Electromagnetics Research B, Vol. 99, 159–178, 2023

A Canonical Filter Theory Approach for the Synthesis of Inductive Wireless Power Systems with Multiple Resonators

Masoud Ahmadi, Tristan VanderMeulen, Loïc Markley*, and Thomas Johnson*

Abstract—The advantage of the canonical filter theory approach to design inductive power transfer (IPT) systems is that values for the coupled resonator elements are readily calculated from scaled canonical filter prototypes with specific frequency response characteristics. For example, Butterworth bandpass filter prototypes can be used to synthesize resonant-coupled IPT systems with critically-coupled frequency response characteristics. In this work, we analyze two canonical filter prototype structures: one prototype has series matching elements at the ports, and the other prototype has shunt matching elements at the ports. Equations are provided to transform the networks into coupled resonator structures that implement IPT links with a transmitter, receiver, and multiple repeater coils. The filter methodology for IPT link synthesis also provides an easy framework to evaluate design trade-offs. An example of comparing resonator inductor sizes for both the series and shunt matching topologies is shown for IPT links operating in ISM frequency bands of 6.78 MHz, 13.56 MHz, 27.12 MHz, and 40.68 MHz. Experimental results are shown for four different IPT examples that were designed using filter synthesis methods.

1. INTRODUCTION

With the surge in battery powered electronic devices, the demand for automated, convenient, fast, and safe charging solutions is greater than ever. Near-field wireless power transfer (WPT) systems have gained interest as a viable method to recharge batteries without the need for power cords and wiring harnesses. The removal of power connectors also enables wireless devices to be completely sealed. Furthermore, WPT systems can automatically detect the presence of a nearby transmitter that enables self-charging features in wireless devices. Applications include wearable electronics [1], implantable medical devices [2, 3], sensor networks [4], autonomous devices such as robots [5], and electric vehicle charging systems [6–8].

In a near-field WPT system, an electromagnetic field is used to couple power from a transmitter to a receiver. A WPT system where the electromagnetic coupling is dominated by a magnetic field is referred to as inductive power transfer (IPT), while a system where the coupling is dominated by electric field coupling is called capacitive power transfer (CPT). In both IPT and CPT, the use of resonators in the transmitter and receiver enhances the electromagnetic field coupling to provide higher efficiency at longer distances.

Various analytic methods have been used to design WPT systems composed of coupled resonators. Most of these methods employ direct circuit analysis techniques for specific network topologies [9–19]. Using direct circuit analysis to find voltage and current in each coil can be tedious and cumbersome, especially for systems with a large number of resonators.

Another method used to design WPT links is based on admittance or impedance inverters that model the coupling between resonators [20–23]. The inverter-based method avoids calculating the

Received 21 November 2022, Accepted 11 January 2023, Scheduled 5 April 2023
* Corresponding authors: Loïc Markley (loic.markley@ubc.ca), Thomas Johnson (thomas.johnson@ubc.ca).
The authors are with the School of Engineering, The University of British Columbia, Kelowna, BC, Canada.

voltage and current in each coil, significantly simplifying the analysis. The inverter-based method is concise in comparison to the direct circuit analysis. However, the drawback of the inverter design methodology is that it is iterative, and several design cycles may be required to determine the values of the inverter impedances for a given source and load impedance. A limitation of both direct circuit analysis and inverter analysis is that the methodology focuses on synthesizing a coupling network for a specific operating frequency, and these methods do not provide analytic tools for including the synthesis of coupling networks with a prescribed frequency response.

A third method that can be used to incorporate frequency response is to visualize the coupling network as a filter [24–27]. Matching the expression for the power efficiency of a link to a filter transfer function enables the design of a specific frequency response. In particular, filter design from canonical prototypes offers a distinctly different approach from the synthesis of matched WPT links that includes a general, systematic, and diverse range of canonical network structures that can be matched for specific terminal impedances and specific frequency response characteristics. By using well-known prototype network structures, specific component values can be computed without the need for detailed circuit analysis by using standard tables of filter coefficients for a specific type of frequency response. Filter theory also provides other analytically tractable methods to evaluate the impact of finite resonator Q on the insertion loss of IPT networks.

The synthesis of matched resonators for critically-coupled WPT links using Butterworth filter prototypes was first investigated in [28]. In this work, the synthesis procedure begins with a canonical filter prototype that is transformed into a network of coupled resonators where impedance inverters are used to implement the coupling. In this way, the transformed network can be directly related to the physical geometry of the transmission link. Subsequent investigations [29–31] focused on transforming a second-order Butterworth bandpass filter prototype into a network where two identical series resonators are coupled. Other works [32, 33] extended the application of filter theory to the synthesis of series resonator IPT links with an arbitrary number of identical and non-identical resonators.

In previous studies using canonical filter theory concepts to synthesize IPT links, the circuits use series resonators as the first and last network elements. We refer to this configuration as a series-series IPT network and refer to intermediate resonators as repeaters. Another network topology that can be synthesized is a shunt-shunt network where the first and last resonators are shunt (parallel) resonators that couple to repeater resonators. The synthesis of shunt-shunt IPT resonator structures has not been described before and will be the primary focus of this paper.

Here we expand the application of canonical filter theory to synthesize IPT systems with an arbitrary number of resonators arranged in a shunt-shunt configuration. It is shown that for systems with three or more resonators, additional approximations are required to synthesize the final network with coupled resonators. As a consequence of these approximations, the frequency response of higher-order systems deviates from the ideal response through small changes to the in-band ripple and an expansion of the bandwidth. Expressions for calculating circuit element values are tabulated for systems up to five resonators. The shunt-shunt synthesis methodology is compared with the series-series synthesis methodology, and guidelines are provided to select an appropriate topology for IPT systems operating in ISM bands from 6.78 MHz to 40.68 MHz. Examples of both shunt-shunt and series-series IPT links are given. These examples include experimental results as well as theoretical estimates of the impact of finite resonator Q. The extension to shunt-shunt coupling structures expands the utility of the filter synthesis method as a way of directly synthesizing IPT coupling networks that meet requirements such as achieving specific terminal impedances or providing a particular frequency response profile.

2. SYNTHESIS FROM FILTER PROTOTYPES

In this section, we begin our analysis by working through steps to transform a bandpass filter into an equivalent circuit composed of inductively coupled resonators. The synthesis starts with a canonical low-pass filter prototype circuit that has a maximally flat frequency response.

Normalized values of the circuit elements are tabulated in filter design tables for low-pass filters with specific types of frequency response characteristics such as maximally flat (Butterworth) responses or equi-ripple (Chebyshev) responses. The filter order (N) determines the number of reactive elements in the network, and the normalized component values are identified as $g_0, g_1, \ldots, g_{N+1}$. The reactive

components are g_1 through g_N; the source resistance is g_0; and the load resistance is g_{N+1}.

Low-pass filter prototypes are synthesized with either a current source or a voltage source input. The reactive network of the filter with a current source input begins with a shunt capacitor, while the first reactive element in the filter network with a voltage source is a series inductor. The terms shunt and series are used to distinguish between these two types of network topologies.

Frequency and impedance scaling is used to transform the low-pass canonical prototype into a bandpass filter by replacing each reactive element with an LC resonator [34]. The bandpass filter network is then converted into a network of mutually coupled resonators using impedance or admittance inverters. Our goal is to have a general approach for designing IPT links with N resonators, where the link has matched termination impedances with predictable frequency response characteristics, and the link can be implemented in either series-series and shunt-shunt network configurations.

2.1. Series-Series Resonator Coupling

We first go through the synthesis of matched IPT links with series elements at the port terminations. Although the synthesis of series-series filter networks for IPT applications has been described in the literature [32, 33], we generalize the design equations and present them in a way that is easily compared with the subsequent analysis of shunt-shunt networks.

As an initial example of a series-series IPT resonator network, consider the transformation of a third-order filter network. Generalized expressions for the transformation of an Nth-order filter prototype are provided at the end of this section. The third-order bandpass filter prototype is shown in Fig. 1(a). The filter elements are

$$\begin{aligned} R_{0,\mathrm{S}} &= \frac{k_\mathrm{z}}{g_0} \qquad R_{4,\mathrm{S}} = k_\mathrm{z}\, g_4 \\ L_{1,\mathrm{S}} &= \frac{k_\mathrm{z}\, g_1}{\omega_b} \quad C_{1,\mathrm{S}} = \frac{1}{\omega_o^2\, L_{1,\mathrm{S}}} \\ C_{2,\mathrm{S}} &= \frac{g_2}{k_\mathrm{z}\, \omega_b} \quad L_{2,\mathrm{S}} = \frac{1}{\omega_o^2\, C_{2,\mathrm{S}}} \\ L_{3,\mathrm{S}} &= \frac{k_\mathrm{z}\, g_3}{\omega_b} \quad C_{3,\mathrm{S}} = \frac{1}{\omega_o^2\, L_{3,\mathrm{S}}}, \end{aligned} \tag{1}$$

where ω_o is the center frequency, k_z the impedance scaling factor, and ω_b the frequency bandwidth. It is also useful to define the normalized frequency bandwidth as $\Delta = \omega_b/\omega_o$. The subscript "S" in (1) denotes that the filter prototype begins with a series resonator.

In the first transformation step, two impedance inverters are added to change the shunt resonator $L_{2,\mathrm{S}}\, C_{2,\mathrm{S}}$ into a series resonator as shown in Fig. 1(a). The series resonator has an inductor value $m_{21} L_{1,\mathrm{S}}$ and a capacitor value $C_{1,\mathrm{S}}/m_{21}$, where m_{21} is a resonator scaling factor that allows the elements of the second resonator to be scaled with respect to the element values of the first resonator. More generally, the elements of an Nth order system are scaled by m_{j1}, where $j = 2, 3, 4, \ldots, N$. The subscript notation "$j1$" means that the scaling of the jth resonator is with reference to the elements in the first resonator. Note that the resonator scaling factors do not change the resonant frequency of the resonator, and the scaling factor is included as a means of adjusting the values (sizes) of the resonator components. Using the scale factor m_{21}, the corresponding inverter impedance in Fig. 1(a) is

$$K_{1,\mathrm{S}} = K_{2,\mathrm{S}} = \sqrt{\frac{m_{21} L_{1,\mathrm{S}}}{C_{2,\mathrm{S}}}} = k_\mathrm{z} \sqrt{\frac{m_{21} g_1}{g_2}}. \tag{2}$$

In the second transformation step shown in Fig. 1(b), the third resonator element values are scaled to match the first resonator element values. The transformation is made by adding a redundant inverter $K_{3,\mathrm{S}}$ to the output port of the filter. The corresponding impedance of the redundant inverter is

$$K_{3,\mathrm{S}} = R_{4,\mathrm{S}} = k_\mathrm{z}\, g_4. \tag{3}$$

After adding the redundant inverter, the third resonator can be re-scaled by m_{31} with reference to the element values of the first resonator. The re-scaled resonator network is shown in Fig. 1(c) where

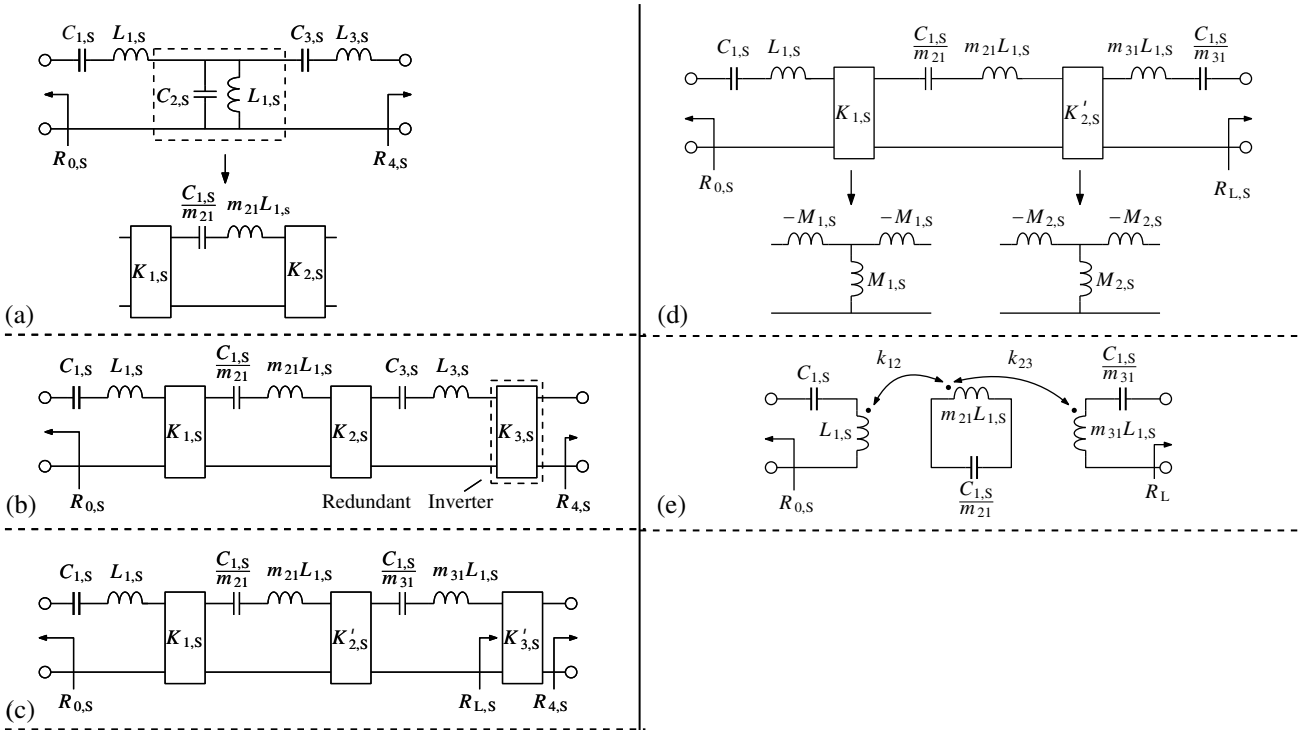

Figure 1. A third-order filter prototype is shown in (a). Impedance inverters are used to transform the shunt resonator into a series resonator in (b). The elements of the third resonator are scaled with respect to the capacitance and inductance of the first resonator in (c). The impedance inverters are replaced with their lumped-element equivalent circuit consisting of a T-network of inductances in (d). The final transformed network with series-series resonator coupling is shown in (e).

the second and third inverters impedances are

$$K'_{2,\mathrm{S}} = K_{2,\mathrm{S}}\sqrt{\frac{m_{31}\,L_{1,\mathrm{S}}}{L_{3,\mathrm{S}}}} = k_{\mathrm{z}}\,g_1\sqrt{\frac{m_{31}m_{21}}{g_2 g_3}} \tag{4a}$$

$$K'_{3,\mathrm{S}} = K_{3,\mathrm{S}}\sqrt{\frac{m_{31}L_{1,\mathrm{S}}}{L_{3,\mathrm{S}}}} = k_{\mathrm{z}}\,g_4\sqrt{\frac{m_{31}g_1}{g_3}} \tag{4b}$$

The third impedance inverter $K'_{3,\mathrm{S}}$ can be removed from the network by changing the load resistance from $R_{4,S}$ to

$$R_{L,\mathrm{S}} = \frac{(K'_{3,\mathrm{S}})^2}{R_{4,\mathrm{S}}} = \frac{m_{31}\,k_{\mathrm{z}}\,g_1\,g_4}{g_3}. \tag{5}$$

The network with the readjusted load resistance is shown in Fig. 1(d).

The inverters can be replaced by a lumped-element equivalent circuit consisting of a T-network of inductors as shown in Fig. 1(d). This equivalence is exact at the resonance frequency, but introduces some deviations from the ideal inverter model as the frequency moves away from resonance. Mutual inductances $M_{1,\mathrm{S}}$ and $M_{2,\mathrm{S}}$ are related to the impedance of the inverters as

$$M_{1,\mathrm{S}} = \frac{K_{1,\mathrm{S}}}{\omega_o} \tag{6a}$$

$$M_{2,\mathrm{S}} = \frac{K'_{2,\mathrm{S}}}{\omega_o}. \tag{6b}$$

Since mutually coupled inductors can also be modelled by an equivalent T-network of inductors, the circuit is simplified to a network of coupled resonators as shown in Fig. 1(e). Note that this transformation is possible because the middle resonator's inductor is connected in series with the mutual inductors representing the voltage contributions from the adjacent coupled resonators. Expressions for the resonator coupling coefficients are derived from the T-model as

$$k_{12} = \frac{M_{1,\mathrm{S}}}{L_{1,\mathrm{S}}\sqrt{m_{21}}} = \frac{\Delta}{\sqrt{g_1 g_2}} \tag{7a}$$

$$k_{23} = \frac{M_{2,\mathrm{S}}}{L_{1,\mathrm{S}}\sqrt{m_{31}}} = \frac{\Delta}{\sqrt{g_2 g_3}}. \tag{7b}$$

Our synthesis of an IPT link is now complete, and a third-order filter prototype is transformed into a network with series-series resonant coupling.

Note that the circuit model in Fig. 1(e) does not include cross coupling between the transmitter inductance $L_{1,S}$ and receiver inductance $m_{31}L_{1,S}$. Neglecting cross-coupling terms at the initial design phase for higher-order WPT systems is common and significantly reduces the complexity of deriving general expressions [20, 21, 33, 35]. Moreover, a careful design of the physical geometry of the coils can minimize the impact of cross-coupling between non-adjacent resonators.

The canonical filter theory method can be expanded to design IPT links with multiple resonators, as shown in Fig. 2. For an Nth-order filter prototype, the design equations are as follows:

$$L_{i,\mathrm{S}} = \begin{cases} \dfrac{k_{\mathrm{z}}\, g_i}{\omega_b}, & \text{if } i \text{ odd} \\ \dfrac{1}{\omega_o^2\, C_{i,\mathrm{S}}}, & \text{if } i \text{ even} \end{cases} \tag{8a}$$

$$C_{i,\mathrm{S}} = \begin{cases} \dfrac{1}{\omega_o^2\, L_{i,\mathrm{S}}}, & \text{if } i \text{ odd} \\ \dfrac{g_i}{k_{\mathrm{z}}\, \omega_b}, & \text{if } i \text{ even} \end{cases} \tag{8b}$$

$$R_{0,\mathrm{S}} = \frac{k_{\mathrm{z}}}{g_0} \tag{8c}$$

$$R_{(N+1),\mathrm{S}} = k_{\mathrm{z}}\, g_{N+1}, \tag{8d}$$

$$R_{\mathrm{L,S}} = \begin{cases} \dfrac{k_{\mathrm{z}}\, m_{N1}\, g_1\, g_{N+1}}{g_N}, & \text{if } N \text{ odd} \\ \dfrac{k_{\mathrm{z}}\, m_{N1}\, g_1}{g_N\, g_{N+1}}, & \text{if } N \text{ even} \end{cases} \tag{8e}$$

$$k_{(j-1)(j)} = \frac{\Delta}{\sqrt{g_{j-1}\, g_j}}. \tag{8f}$$

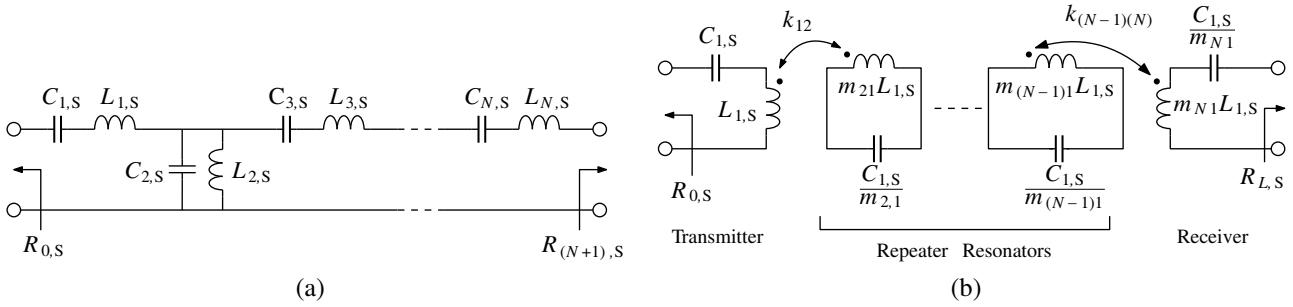

Figure 2. The general bandpass filter prototype with N resonators is shown in (a). The transformed filter with series-series resonator coupling is shown in (b).

For these equations, i and j are indices that range from 1 through N and $i \neq j$. In the transformed network shown in Fig. 2(b), the inductances of the repeater and receiver coils are scaled with respect to the transmitter coil by scaling factors m_{j1}, for $j = 2, 3, 4, \ldots, N$. For example, when $m_{j1} = 1$, all resonators in the IPT network are identical. The capacitances in the resonators are also scaled, and scaling provides additional flexibility to synthesize IPT links with different coil sizes.

2.2. Shunt-Shunt Resonator Coupling

In the previous section, canonical filter prototype networks were transformed into IPT links with a series capacitor for matching the first and last coils, creating series resonator structures at the transmitting and receiving ports. In this section, the methodology is extended to include the synthesis of IPT links that have a shunt (parallel) capacitor for matching the first and last coils. Shunt matching produces shunt resonator circuits at the input and output ports. We will refer to this configuration as shunt-shunt resonator coupling. The subscript 'P' is used throughout this work to differentiate the shunt resonator network configuration from the series resonator configuration (identified by the subscript 'S').

Similar to the previous analysis, let's begin with a third-order example and then generalize to Nth-order filter prototypes.

The third-order filter prototype is shown in Fig. 3(a), and the circuit element values are:

$$\begin{aligned} R_{0,\mathrm{P}} &= k_\mathrm{z}\, g_0 & R_{4,\mathrm{P}} &= k_\mathrm{z}\, g_4 \\ C_{1,\mathrm{P}} &= \frac{g_1}{k_\mathrm{z}\,\omega_b} & L_{1,\mathrm{P}} &= \frac{1}{\omega_o^2\, C_{1,\mathrm{P}}} \\ L_{2,\mathrm{P}} &= \frac{k_\mathrm{z}\, g_2}{\omega_b} & C_{2,\mathrm{P}} &= \frac{1}{\omega_o^2\, L_{2,\mathrm{P}}} \\ C_{3,\mathrm{P}} &= \frac{g_3}{k_\mathrm{z}\,\omega_b} & L_{3,\mathrm{P}} &= \frac{1}{\omega_o^2\, C_{3,\mathrm{P}}}. \end{aligned} \tag{9}$$

In the first step, impedance inverters $K_{1,\mathrm{P}}$ and $K_{2,\mathrm{P}}$ are used to convert the series resonator into a shunt resonator as shown in Fig. 3(b). For this transformation step, the inverter impedances are

$$K_{1,\mathrm{P}} = K_{2,\mathrm{P}} = \sqrt{\frac{m_{21} L_{2,\mathrm{P}}}{C_{1,\mathrm{P}}}} = k_\mathrm{z}\sqrt{\frac{m_{21} g_2}{g_1}}. \tag{10}$$

In the second step, a redundant inverter ($K_{3,\mathrm{P}}$) is added to the output of the filter as shown in Fig. 3(c). The redundant inverter provides a way to scale the values of the third resonator. The impedance of the redundant inverter is

$$K_{3,\mathrm{P}} = R_{4,\mathrm{P}} = k_\mathrm{z} g_4. \tag{11}$$

We can now change the impedance level of the third resonator to $m_{31}\sqrt{L_{1,\mathrm{P}}/C_{1,\mathrm{P}}}$ by modifying the second and third inverter impedances. The re-scaled inverters are

$$K'_{2,\mathrm{P}} = K_{2,\mathrm{P}}\sqrt{\frac{m_{31} C_{3,\mathrm{P}}}{C_{1,\mathrm{P}}}} = \frac{k_\mathrm{z}}{g_1}\sqrt{m_{31} m_{21} g_2 g_3} \tag{12a}$$

$$K'_{3,\mathrm{P}} = K_{3,\mathrm{P}}\sqrt{\frac{m_{31} C_{3,\mathrm{P}}}{C_{1,\mathrm{P}}}} = k_\mathrm{z} g_4\sqrt{\frac{m_{31} g_3}{g_1}}. \tag{12b}$$

The resultant network is shown in Fig. 3(c). In the next step shown in Fig. 3(d), the redundant inverter $K'_{3,\mathrm{P}}$ is absorbed into an equivalent load resistance $R_{L,\mathrm{P}}$ where

$$R_{L,\mathrm{P}} = \frac{(K'_{3,\mathrm{P}})^2}{R_{4,\mathrm{P}}} = \frac{m_{31}\, k_\mathrm{z}\, g_3\, g_4}{g_1}. \tag{13}$$

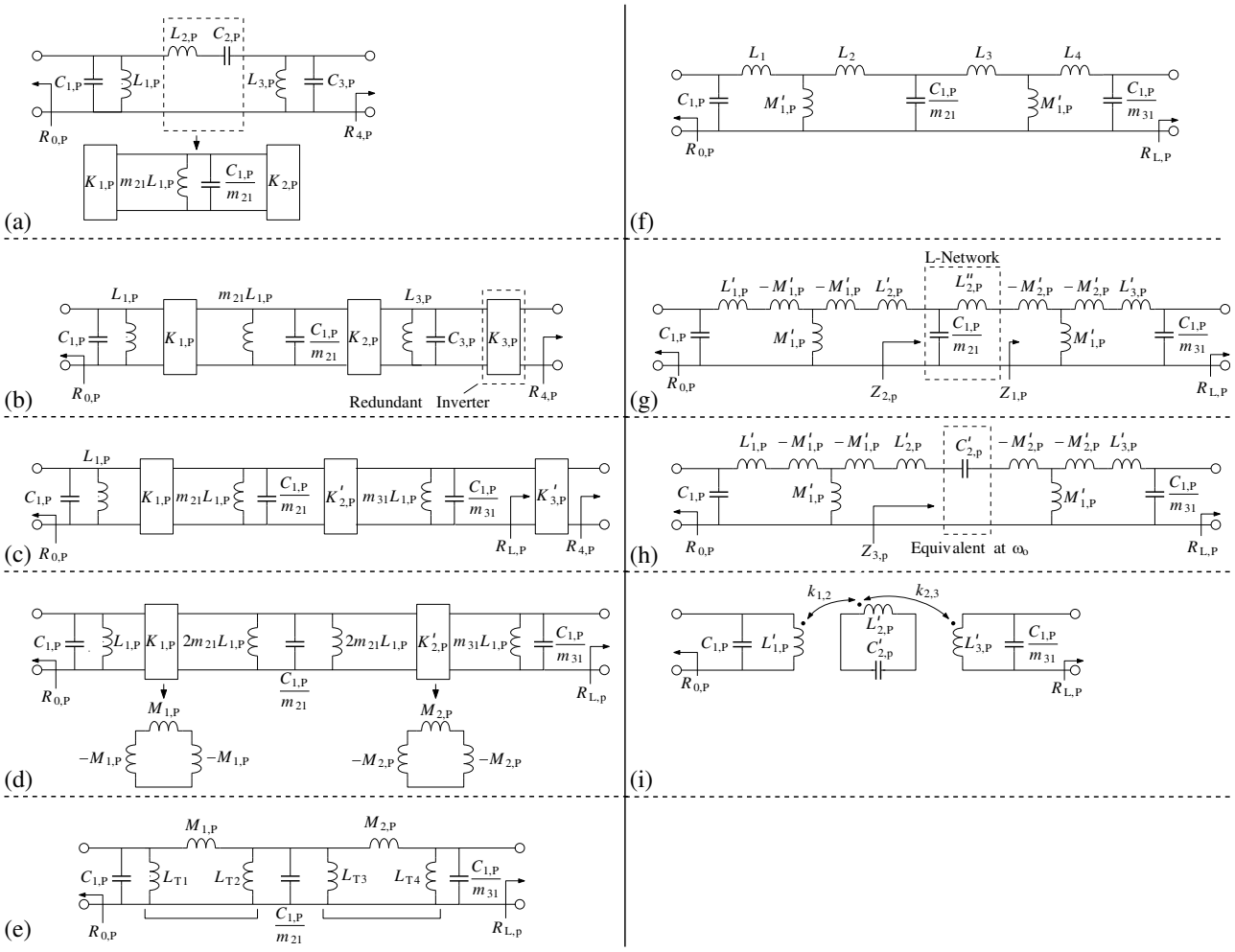

Figure 3. The transformation of a third-order filter network into a circuit with shunt-shunt resonator coupling is shown. Inverters are used to convert the series resonator to a shunt resonator in (a). In (b), a redundant inverter is added to the load. The impedance level of the third resonator is scaled in (c). In (d), the third inverter is absorbed into an equivalent load resistance and the inverters are replaced by a lumped-element equivalent network. Inductors are consolidated in (e). Π-networks of inductances converted to T-networks using Δ-Y transformation in (f). The series inductances are partitioned to form mutually coupled inductors in (g). The L-network is approximated by an equivalent series capacitance at ω_o in (h). The final transformed network is shown in (i).

The filter circuit shown in Fig. 3(c) still requires additional steps to replace the ideal impedance inverters with coupled coils. The ideal impedance inverters are replaced with equivalent finite bandwidth impedance inverters consisting of Π-networks of inductors where

$$M_{1,\mathrm{P}} = \frac{K_{1,\mathrm{P}}}{\omega_o} \tag{14a}$$

$$M_{2,\mathrm{P}} = \frac{K'_{2,\mathrm{P}}}{\omega_o} \tag{14b}$$

In addition to the impedance inverter transformation, the inductor $m_{21}L_{1,\mathrm{P}}$ in Fig. 3(c) is also split into two parallel inductors, each with a value of $2m_{21}L_{1,\mathrm{P}}$. The partitioning of the inductor into two parallel inductors is made in anticipation of the next step shown in Fig. 3(e) where the shunt inductances on

each side of $M_{1,\mathrm{P}}$ and $M_{2,\mathrm{P}}$ are consolidated into equivalent inductances such that

$$L_{T1} = \frac{M_{1,\mathrm{P}}\, L_{1,\mathrm{P}}}{M_{1,\mathrm{P}} - L_{1,\mathrm{P}}} \tag{15a}$$

$$L_{T2} = \frac{2m_{21} M_{1,\mathrm{P}}\, L_{1,\mathrm{P}}}{M_{1,\mathrm{P}} - 2m_{21}\, L_{1,\mathrm{P}}} \tag{15b}$$

$$L_{T3} = \frac{2m_{21} M_{2,\mathrm{P}}\, L_{1,\mathrm{P}}}{M_{2,\mathrm{P}} - 2m_{21}\, L_{1,\mathrm{P}}} \tag{15c}$$

$$L_{T4} = \frac{2\, m_{31} M_{2,\mathrm{P}}\, L_{1,\mathrm{P}}}{M_{2,\mathrm{P}} - 2m_{31}\, L_{1,\mathrm{P}}}, \tag{15d}$$

After using these equations, the circuit in Fig. 3(e) has a middle resonator composed of two shunt inductors L_{T2} and L_{T3} that couple separately to the transmitter and receiver coils, respectively.

In the next step, the Π-networks of inductors are replaced by an equivalent T-network using a Δ-Y transformation as shown in circuit Fig. 3(f). The series inductances L_1, L_2, L_3, and L_4 are subsequently partitioned into two series inductances, one of which is equal to $M'_{1,\mathrm{P}}$ and the other equal to $M'_{2,\mathrm{P}}$ as seen in Fig. 3(g). In this circuit, we have

$$L'_{1,\mathrm{P}} = \frac{\Delta\, k_{\mathrm{z}}\, g_2}{\omega_o(g_1\, g_2 - 2\Delta^2)} \tag{16a}$$

$$L'_{2,\mathrm{P}} = \frac{2\Delta\, k_{\mathrm{z}}\, g_2\, m_{21}}{\omega_o(g_1\, g_2 - 2\Delta^2)} \tag{16b}$$

$$L''_{2,\mathrm{P}} = \frac{2\Delta\, k_{\mathrm{z}}\, g_2\, g_3\, m_{21}}{g_1\omega_o(g_2\, g_3 - 2\Delta^2)} \tag{16c}$$

$$L'_{3,\mathrm{P}} = \frac{\Delta\, k_{\mathrm{z}}\, g_2\, g_3\, m_{31}}{\omega_o(g_1\, g_2 - 2\Delta^2)}. \tag{16d}$$

At this point in the analysis, we want to transform the circuit in Fig. 3(g) into three inductively coupled resonators shown in Fig. 3(i). We see that the middle resonator in Fig. 3(g) has two inductors, $L'_{2,\mathrm{P}}$ and $L''_{2,\mathrm{P}}$, that couple separately to the transmitting and receiving resonators. In this configuration, the circuit cannot be physically realized by three coupled resonators, since the middle resonator is composed of two parallel inductors, each independently coupled to an adjacent resonator. If the L-network marked in circuit (g) is capacitive at the center frequency, it can be replaced by an equivalent series capacitance $C'_{2,\mathrm{P}}$ as shown in Fig. 3(h). In this way, a physically realizable resonator is constructed that simultaneously couples to both the transmitting and receiving resonators.

The equivalence of circuits in Figs. 3(g) and (h) requires that the impedance at ω_o seen through the L-network, $Z_{2,\mathrm{P}}$, is the same as the equivalent impedance of the series capacitance, $Z_{3,\mathrm{P}}$. Therefore, we require $Z_{2,\mathrm{P}} = Z_{3,\mathrm{P}}$ at ω_o and find

$$C'_{2,\mathrm{P}} = \frac{g_1\left(g_2\, g_3 - 2\,\Delta^2\right)\,\left(4\,\Delta^2\, {g_4}^2 + {g_2}^2\right)}{2\,\Delta\, g_2\, \mathrm{k_z}\, m_{21}\, \omega_o\,\left({g_2}^2\, g_3 - 4\Delta^2(g_2 + \, g_3\, {g_4}^2)\right)}. \tag{17}$$

It is clear from (2.2) and (17) that we require $\Delta < \min\left[\sqrt{g_2^2\, g_3/4(g_3\, g_4^2 + g_2)}, \sqrt{\dfrac{g_2\, g_3}{2}}\right]$ for the system to be realizable. As shown by examples later, practical WPT systems are typically narrowband, and this condition is easily met. Furthermore, the equality in (17) is valid at the center frequency ω_o and small deviations at other frequencies within the desired bandwidth are expected.

With this approximation, we can now finalize our transformation with the network shown in Fig. 3(i) where the repeater coil is simultaneously coupled to the shunt resonators in the transmitter and receiver. The coupling coefficients in the final network are defined as

$$k_{12} = \frac{M'_{1,\mathrm{P}}}{\sqrt{L'_{1,\mathrm{P}}\, L'_{2,\mathrm{P}}}} = \frac{\sqrt{2}\,\Delta}{\sqrt{g_1\, g_2}} \tag{18a}$$

$$k_{23} = \frac{M'_{2,\mathrm{P}}}{\sqrt{L'_{2,\mathrm{P}}\, L'_{3,\mathrm{P}}}} = \frac{\sqrt{2}\,\Delta}{\sqrt{g_2\, g_3}} \tag{18b}$$

The coupling coefficients of the final network with shunt-shunt resonator coupling are multiplied by a factor of $\sqrt{2}$ compared to those for the network with series-series resonator topology in (7). The modest increase in the coupling coefficient is a consequence of an increase in the frequency bandwidth of the final synthesized network as shown later. With the steps shown in Fig. 3, our synthesis is now complete.

The methodology to synthesize third-order IPT systems can be extended to higher order systems. A general Nth-order filter prototype is shown in Fig. 4(a). The network elements in the filter prototype are

$$C_{i,\mathrm{P}} = \begin{cases} \dfrac{g_i}{k_{\mathrm{z}}\,\omega_b}, & \text{if } i \text{ odd} \\ \dfrac{1}{\omega_o^2\, L_{i,\mathrm{P}}}, & \text{if } i \text{ even} \end{cases} \tag{19a}$$

$$L_{i,\mathrm{P}} = \begin{cases} \dfrac{1}{\omega_o^2\, C_{i,\mathrm{P}}}, & \text{if } i \text{ odd} \\ \dfrac{k_{\mathrm{z}}\, g_i}{\omega_b}, & \text{if } i \text{ even} \end{cases} \tag{19b}$$

$$R_{0,\mathrm{P}} = k_{\mathrm{z}}\, g_0 \tag{19c}$$

$$R_{(N+1),\mathrm{P}} = k_{\mathrm{z}}\, g_{N+1}. \tag{19d}$$

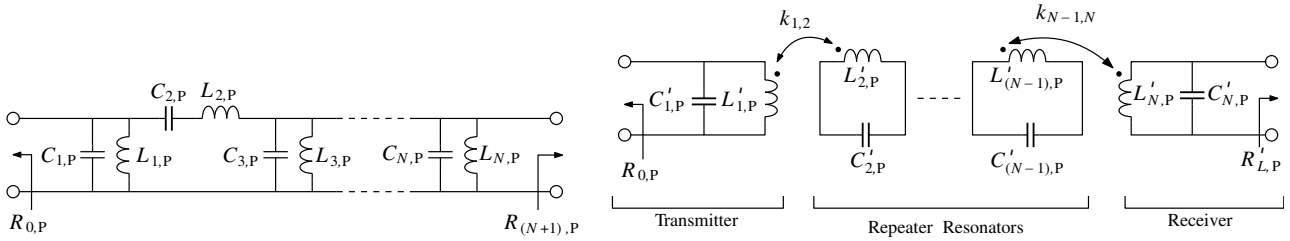

Figure 4. The general bandpass filter prototype with N resonators is shown in (a). The final transformed filter network with shunt resonators at the input and output ports is shown in (b). The intermediate resonators in (b) are the repeaters.

The equivalent IPT network with shunt-shunt resonator coupling is shown in Fig. 4(b). The values of the reactive elements are shown in Tables 1 and 2 for orders up to five. The coupling between adjacent resonators is given by

$$k_{(j-1)(j)} = \frac{\sqrt{2}\,\Delta}{\sqrt{g_{j-1}\, g_j}}. \tag{20}$$

Note that (20) is valid for $N > 2$; for $N = 2$, there are no repeater coils, and the coupling coefficient is $\Delta/\sqrt{g_1\, g_2}$, similar to (8f) for series-series resonator coupling. The equivalent load resistances for even and odd order configurations are

$$R_{L,\mathrm{P}} = \begin{cases} \dfrac{k_{\mathrm{z}}\, m_{N,1}\, g_N\, g_{N+1}}{g_1}, & \text{if } N \text{ odd} \\ \dfrac{k_{\mathrm{z}}\, m_{N,1}\, g_N}{g_1\, g_{N+1}}, & \text{if } N \text{ even} \end{cases} \tag{21}$$

Table 1. Resonator inductance expressions for IPT networks with shunt-shunt resonator port terminations.

N	$L'_{1,\mathrm{P}}$	$L'_{2,\mathrm{P}}$	$L'_{3,\mathrm{P}}$	$L'_{4,\mathrm{P}}$	L'_{5p}
2	$\frac{g_2\,\mathrm{k_z}\,\Delta}{\omega_o\,(g_1\,g_2-\Delta^2)}$	$\frac{g_2\,\mathrm{k_z}\,\Delta\,m_{21}}{\omega_o\,(g_1\,g_2-\Delta^2)}$			
3	$\frac{g_2\,\mathrm{k_z}\,\Delta}{\omega_o\,(g_1\,g_2-2\,\Delta^2)}$	$\frac{2\,g_2\,\mathrm{k_z}\,\Delta\,m_{21}}{\omega_o\,(g_1\,g_2-2\,\Delta^2)}$	$\frac{g_2\,g_3\,\mathrm{k_z}\,\Delta\,m_{31}}{g_1\,\omega_o\,(g_2\,g_3-2\,\Delta^2)}$		
4	$\frac{g_2\,\mathrm{k_z}\,\Delta}{\omega_o\,(g_1\,g_2-2\,\Delta^2)}$	$\frac{2\,g_2\,\mathrm{k_z}\,\Delta\,m_{21}}{\omega_o\,(g_1\,g_2-2\,\Delta^2)}$	$\frac{2\,g_2\,g_3\,\mathrm{k_z}\,\Delta\,m_{31}}{g_1\,\omega_o\,(g_2\,g_3-4\,\Delta^2)}$	$\frac{g_3\,g_4\,\mathrm{k_z}\,\Delta\,m_{4,1}}{g_1\,\omega_o\,(g_3\,g_4-2\,\Delta^2)}$	
5	$\frac{g_2\,\mathrm{k_z}\,\Delta}{\omega_o\,(g_1\,g_2-2\,\Delta^2)}$	$\frac{2\,g_2\,\mathrm{k_z}\,\Delta\,m_{21}}{\omega_o\,(g_1\,g_2-2\,\Delta^2)}$	$\frac{2\,g_2\,g_3\,\mathrm{k_z}\,\Delta\,m_{31}}{g_1\,\omega_o\,(g_2\,g_3-4\,\Delta^2)}$	$\frac{2\,g_3\,g_4\,\mathrm{k_z}\,\Delta\,m_{4,1}}{g_1\,\omega_o\,(g_3\,g_4-4\,\Delta^2)}$	$\frac{g_4\,g_5\,\mathrm{k_z}\,\Delta\,m_{5,1}}{g_1\,\omega_o\,(g_4\,g_5-2\,\Delta^2)}$

Table 2. Resonator capacitance expressions for IPT networks with shunt-shunt resonator port terminations.

N	$C'_{1,\mathrm{P}}$	$C'_{2,\mathrm{P}}$	$C'_{3,\mathrm{P}}$
2	$\frac{g_1}{\mathrm{k_z}\,\omega_b}$	$\frac{g_1}{\mathrm{k_z}\,\omega_b\,m_{21}}$	
3	$\frac{g_1}{\mathrm{k_z}\,\omega_b}$	$\frac{g_1\,\left(g_2\,g_3-2\,\Delta^2\right)\,\left(4\,{g_4}^2\,\Delta^2+{g_2}^2\right)}{2\,g_2\,\mathrm{k_z}\,\omega_b\,m_{21}\,({g_2}^2\,g_3-4\Delta^2(g_2+\,g_3\,{g_4}^2))}$	$\frac{g_1}{\mathrm{k_z}\,m_{31}\,\omega_b}$
4	$\frac{g_1}{\mathrm{k_z}\,\omega_b}$	$\frac{g_1\,\left(g_2\,g_3-4\,\Delta^2\right)\,\left({g_2}^2+4\,{g_5}^2\,\Delta^2\right)}{2\,g_2\,\mathrm{kz}\,\omega_b\,m_{21}\,({g_2}^2\,g_3-4\,\Delta^2\,(2\,g_2+\,g_3\,{g_5}^2))}$	$\frac{g_1\,\left(g_3\,g_4-2\,\Delta^2\right)\,\left(4\,\Delta^2+{g_3}^2\,{g_5}^2\right)}{2\,g_3\,\mathrm{k_z}\,\omega_b\,m_{31}\,({g_3}^2\,g_4\,{g_5}^2-4\,\Delta^2(g_4+\,g_3\,{g_5}^2))}$
5	$\frac{g_1}{\mathrm{k_z}\,\omega_b}$	$\frac{g_1\,\left(g_2\,g_3-4\,\Delta^2\right)\,\left({g_2}^2+4\,{g_6}^2\,\Delta^2\right)}{2g_2\,\mathrm{kz}\,\omega_b\,m_{21}\,({g_2}^2\,g_3-4\,\Delta^2(2\,g_2+g_3\,{g_6}^2))}$	$\frac{g_1\,\left(g_3\,g_4-2\,\Delta^2\right)\,\left(4\,\Delta^2+{g_3}^2\,{g_6}^2\right)}{2\,g_3\,\mathrm{k_z}\,\omega_b\,m_{31}\,({g_3}^2\,g_4\,{g_6}^2-4\,\Delta^2(g_4+\,g_3\,{g_6}^2))}$

N	$C'_{4,\mathrm{P}}$	C'_{5p}
4	$\frac{g_1}{\mathrm{k_z}\,m_{4,1}\,\omega_b}$	
5	$\frac{g_1\,\left(g_4\,g_5-2\,\Delta^2\right)\,\left({g_4}^2+4\,{g_6}^2\,\Delta^2\right)}{2\,g_4\,\mathrm{k_z}\,\omega_b\,m_{41}\,({g_4}^2\,g_5-4\Delta^2(g_4+\,g_5{g_6}^2))}$	$\frac{g_1}{\mathrm{k_z}\,m_{5,1}\,\omega_b}$

Although the expressions given in Tables 1 and 2 are accurate and have no mismatch loss at the center frequency, there are useful approximations that can be made to simplify the expressions. Since WPT links are narrowband (i.e., $\Delta^2 \ll 1$), the denominator term for the inductor values shown in Table 1 can be simplified by neglecting the Δ^2 term. Simplified expressions for inductances are given in Table 3. The corresponding resonator capacitances using the simplified inductance expressions are given by $C'_{N,\mathrm{P}} = \left(\omega_o^2\,L'_{N,\mathrm{P}}\right)^{-1}$. Further, the capacitance and inductance of the repeater and receiving coils can be scaled with respect to those in the transmitter resonator by a factor of $2m_{j1}$. These expressions are useful for establishing an initial IPT design that can be optimized.

The resonator scaling factors (m_{j1}) can be used to adjust the size of the resonators' components relative to those in the transmitting coil. Later, we show design examples that have repeater coils with a different size from the transmitter and receiver coils, enabling the minimization of cross coupling between coils. The scaling factors are therefore useful for evaluating trade-offs in resonator size and cross-coupling.

Table 3. Simplified expressions for inductances in an IPT network with shunt-shunt resonator port terminations.

N	$L'_{1,\mathrm{P}}$	$L'_{2,\mathrm{P}}$	$L'_{3,\mathrm{P}}$	$L'_{4,\mathrm{P}}$	L'_{5p}
2	$\frac{\mathrm{k_z}\,\Delta}{\omega_o\, g_1}$	$\frac{\mathrm{k_z}\,\Delta\, m_{21}}{\omega_o\, g_1}$			
3	$\frac{\mathrm{k_z}\,\Delta}{\omega_o\, g_1}$	$\frac{2\mathrm{k_z}\,\Delta\, m_{21}}{\omega_o\, g_1}$	$\frac{\mathrm{k_z}\,\Delta\, m_{31}}{\omega_o\, g_1}$		
4	$\frac{\mathrm{k_z}\,\Delta}{\omega_o\, g_1}$	$\frac{2\mathrm{k_z}\,\Delta\, m_{21}}{\omega_o\, g_1}$	$\frac{2\mathrm{k_z}\,\Delta\, m_{31}}{\omega_o\, g_1}$	$\frac{\mathrm{k_z}\,\Delta\, m_{4,1}}{\omega_o\, g_1}$	
5	$\frac{\mathrm{k_z}\,\Delta}{\omega_o\, g_1}$	$\frac{2\mathrm{k_z}\,\Delta\, m_{21}}{\omega_o\, g_1}$	$\frac{2\mathrm{k_z}\,\Delta\, m_{31}}{\omega_o\, g_1}$	$\frac{2\mathrm{k_z}\,\Delta\, m_{4,1}}{\omega_o\, g_1}$	$\frac{\mathrm{k_z}\,\Delta\, m_{5,1}}{\omega_o\, g_1}$

Note that the corresponding capacitance of each resonators is $C'_{N,\mathrm{P}} = \dfrac{1}{\omega_o^2\, L'_{N,\mathrm{P}}}$.

2.3. Filter Losses and Efficiency

The theory described so far has focused on minimizing IPT mismatch losses within a band of frequencies, assuming that all network components are lossless. In practice however, there are dissipative elements in the circuit models for resonators with finite Q that increase in-band attenuation [36–39]. Therefore, the power efficiency of the IPT link is limited by the dissipative components in the network. If finite resonator Q is included in the analysis, the attenuation of the IPT link at the center frequency is approximately [35, 38]

$$A_{\mathrm{dB}} \approx \left[\frac{4.343}{\Delta}\sum_{n=1}^{N}\frac{g_i}{Q_i}\right], \tag{22}$$

where A_{dB} is the loss in dB, and Q_i is the unloaded quality factor of the ith resonator. Equation (22) is derived with the assumption that the filter network is well matched at ω_o so that mismatch loss is minimized. Equation (22) also assumes that the two ports have the same termination resistance. If the IPT network has unequal termination resistances, then the right hand side of (22) must be multiplied by a correction factor

$$F = \frac{4\, g_0\, g_{n+1}}{(g_0 + g_{N+1})^2}, \tag{23}$$

which accounts for unequal termination resistances [36].

3. DESIGN EXAMPLES

We now work through examples of using the filter theory approach to design IPT links. The examples have the following constraints. First, we limit our investigation to doubly-terminated filter networks where the port termination resistance is the same at transmitter and receiver ports. A port termination resistance of 50 Ω is used for all the examples selected to be compatible with the port impedances on the vector network analyzer which was used to verify the designs. Note that the analytic expressions derived in Sections 2.1 and 2.2 are general and can be used to synthesize networks with unequal port termination impedances including singly-terminated networks with ideal voltage sources or ideal current sources. Second, a maximally flat (Butterworth) frequency response is selected for the designs. This response is equivalent to critical coupling. Third, we have selected 27.12 MHz and 40.68 MHz ISM frequency bands for the IPT example. Fourth, the normalized bandwidth is held constant and equal to 0.16.

The first design example is for a second-order series-series resonator IPT link at a frequency of 27.12 MHz. Three other design examples are presented for the shunt-shunt configuration at a frequency of 40.68 MHz. The shunt-shunt examples implement IPT networks corresponding to progressively higher

orders starting with two resonators. Higher order filter networks ($N \geq 3$) have additional degrees of freedom that enable the size of repeater resonator coils to be adjusted relative to the transmitting and receiving coils. In this way, repeater coils that minimize cross-coupling can be selected while maintaining a design that meets specific frequency bandwidth and termination impedance conditions.

The second-order IPT links (series-series and shunt-shunt) are designed to have identical resonators in the transmitter and receiver ($m_{21} = 1$). Using the Butterworth filter coefficients shown in Table 4 and the expressions in Tables 1 and 2, the circuit parameters are calculated and summarized in Table 5. Both second-order links have a coupling coefficient given by $\Delta/\sqrt{g_1 g_2}$ which is equal to 0.1131. Note that the coupling coefficients for the series-series and shunt-shunt cases are only equal for order $N = 2$ as described in Section 2.2.

The third-order IPT link has a shunt-shunt resonator topology and is designed for 40.68 MHz. From (2.2) and (17), $\Delta < 0.5773$ for the link to be physically realizable, which is satisfied by the choice of a 0.16 normalized bandwidth. If a scale factor of 0.5 is used for m_{21}, then the first and second resonators have the same inductance. In this design, we chose a scaling factor of $m_{21} = m_{31} = 1$ such that the repeater coil (middle resonator) has an inductance that is twice as large as the transmitting and receiving coils. Using the filter coefficients in Table 4 and expressions in Table 1 and 2, the circuit parameters are calculated and summarized in Table 5. The coupling coefficients from the transmitter to repeater and repeater to receiver are both 0.16.

Table 4. Butterworth filter coefficients.

N	g_0	g_1	g_2	g_3	g_4	g_5	g_6
2	1.000	1.4142	1.4142	1.0000			
3	1.000	1.0000	2.0000	1.0000	1.0000		
4	1.000	0.7654	1.8478	1.8478	0.7654	1.0000	
5	1.000	0.6180	1.6180	2.0000	1.6180	0.6180	1.0000

Applied Wave Research Microwave Office by Cadence (referred to henceforth as AWR) was used to simulate the third-order IPT link design [40]. The component losses are neglected in the simulation. The transmission response (S_{21}) is shown in Fig. 5(a) and labeled as "Link I". The response of the lumped element filter prototype (Fig. 3(a)) is also shown for comparison and labeled as "Filter Response". At

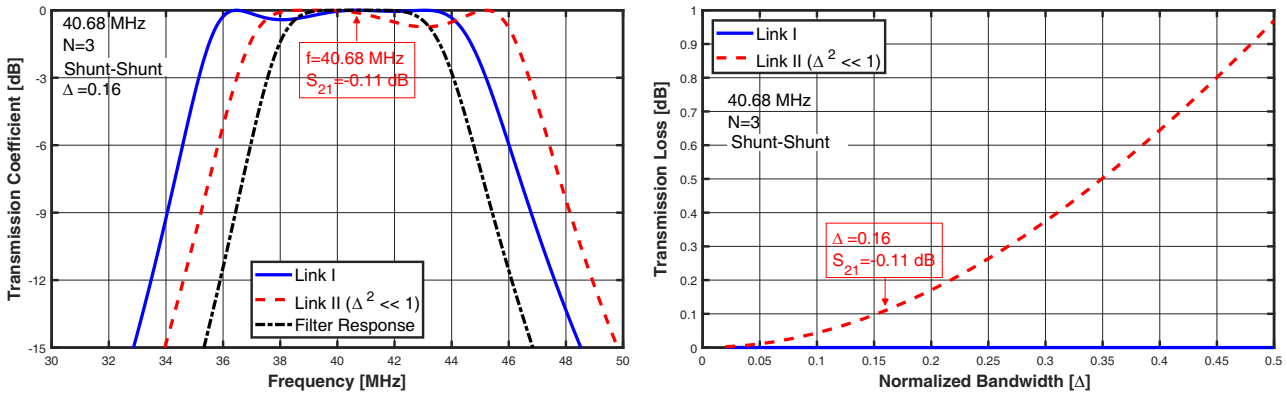

Figure 5. The frequency response of a third-order filter network with different circuit models. The frequency response is shown in (a) and the insertion loss at f_o is shown in (b). The ideal frequency response (circuit in Fig. 3(a)) is labeled as 'Filter Response'. The response for a three resonator IPT link using design equations in Tables 1 and 2 is labelled 'Link I'. The response for a three resonator IPT link using the simplified design equations in Table 3 is labeled as 'Link II'.

the center frequency, both networks are matched to 50 Ω, and the insertion loss is 0 dB. Moving away from the center frequency, the IPT link (Link I) has an in-band dip of 0.42 dB that can be traced back to the synthesis steps where the two-element L-network was approximated with a single series capacitance.

Using the simplified expressions in Table 3, we redesigned the third-order link and called it "Link II". The frequency response of Link II is added to Fig. 5(a). The most notable discrepancy between Link I and Link II is an increased mismatch loss of 0.11 dB (2.5% efficiency loss) at the center frequency. The two links have the same bandwidth expansion; however, unlike Link I, Link II goes through an asymmetric extension around the center frequency.

A more general comparison of the discrepancy between the exact analytic expressions and the simplified expressions for the third-order shunt-shunt resonator configuration is shown in Fig. 5(b). As described in Section 2.2, the simplified expressions neglect all but the lowest order terms in Δ; therefore, we expect to see sensitivity related to bandwidth. The results in Fig. 5(b) confirm this assertion, and we recommend using simplified element expressions over the bandwidth range of $\Delta < 0.10$, where transmission efficiency is maintained above 98%.

Table 5. IPT link design summary. The normalized bandwidth is 0.16, the port resistances are 50 Ω, and the coils have a trace width (w) of 2.5 mm.

Topology N	Parameter	Value	Parameter	Value
series-series	f_o	27.12 MHz	$n_1(n_2)$	4
2	$L_{1,\mathrm{S}}$	2.59 µH	$d_1(d_2)$	6.27 cm
	$C_{1,\mathrm{S}}$	13.30 pF	ℓ_{12}	7.2 cm
	k_{12}	0.1131	S	6.00 mm
	m_{21}	1		
shunt-shunt	f_o	40.68 MHz	$n_1(n_2)$	1
2	$L'_{1,\mathrm{P}}$	22.40 nH	$d_1(d_2)$	1.21 cm
	$C_{1,\mathrm{P}}$	692.0 pF	ℓ_{12}	0.8 cm
	k_{12}	0.113		
	m_{21}	1		
shunt-shunt	f_o	40.68 MHz	$n_1(n_2)$	1
3	$L'_{1,\mathrm{P}}(L'_{3,\mathrm{P}})$	32.20 nH	n_3	1
	$L'_{2,\mathrm{P}}$	64.40 nH	$d_1(d_3)$	1.63 cm
	$C_{1,\mathrm{P}}(C'_{3,\mathrm{P}})$	489.0 pF	d_2	2.90 cm
	$C'_{2,\mathrm{P}}$	250.8 pF	ℓ_{12}	0.8 cm
	$k_{12}(k_{23})$	0.16	ℓ_{23}	0.8 cm
	$m_{21}(m_{31})$	1		
shunt-shunt	f_o	40.68 MHz	$n_1(n_4)$	1
4	$L'_{1,\mathrm{P}}(L'_{4,\mathrm{P}})$	42.34 nH	$n_2(n_3)$	1
	$L'_{2,\mathrm{P}}(L'_{3,\mathrm{P}})$	33.33 nH	$d_1(d_4)$	2.05 cm
	$C_{1,\mathrm{P}}(C'_{4,\mathrm{P}})$	374.0 pF	$d_2(d_3)$	1.69 cm
	$C'_{2,\mathrm{P}}$	513.0 pF	ℓ_{12}	0.8 cm
	$C'_{3,\mathrm{P}}$	520.0 pF	ℓ_{23}	0.8 cm
	$k_{12}(k_{34})$	0.1902	ℓ_{34}	0.8 cm
	k_{23}	0.1224		
	$m_{21}(m_{31})$	0.4		
	$m_{4,1}$	1		

Our last example is a fourth-order IPT link at 40.68 MHz with two repeater coils and shunt-shunt port matching. Using the design equations, the link is physically realizable providing $\Delta < 0.50$, which is easily met by selecting a normalized bandwidth of 0.16. If scaling factors m_{21} and m_{31} are 0.5 and 0.5032, respectively, then all resonator coils have the same inductance. We however chose different scaling factors such that $m_{21} = m_{31} = 0.4$ and $m_{41} = 1$. In this way, the repeater coils have a smaller inductance than the transmitter and receiver coils. The circuit parameters are calculated based on the expressions in Tables 1 and 2, and the design values are summarized in Table 5.

4. A COMPARISON OF SHUNT AND SERIES IPT CONFIGURATIONS

An advantage of using filter theory to design IPT systems is that it is easy to compare different design trade-offs. Filter theory uses canonical networks that can be chosen to have either series or shunt matching topologies and can be easily scaled for changes in impedance and frequency. As an example of exploring design trade-offs, we consider the question of resonator inductor size and make a comparison of the series-series and shunt-shunt port matching topologies.

For the comparison, we use a third-order network with a transmitter, repeater, and receiver coil. The termination resistances are set to 50 Ω, and the frequency response is maximally flat. The two IPT links are designed with identical resonators. This means that $m_{31} = 1$ for both the series and shunt matched links. The other scale factor, m_{21}, is unity for the series-series link and 0.5 for the shunt-shunt link. The design equations are used to calculate $L_{1,\mathrm{S}}$ for the series topology and $L'_{1,\mathrm{P}}$ for the shunt topology as a function of normalized bandwidth (coupling coefficient). The results are shown in Fig. 6 for ISM band frequencies at 6.78 MHz, 13.56 MHz, 27.12 MHz, and 40.68 MHz. For a normalized bandwidth of 10% (0.1), the resonator inductances in the series configuration are two orders of magnitude larger than the shunt configuration. Further, the differences in inductance become significantly larger for normalized bandwidths less than 0.10. These are obtained when coupling is weak, corresponding to larger power transfer distances.

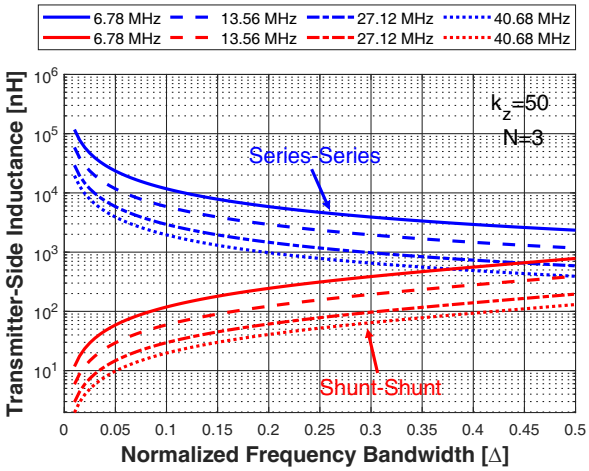

Figure 6. The transmitter inductance is shown versus the normalized frequency bandwidth for both series (blue) and shunt (red). The inductance is plotted for systems operating at four different ISM bands.

For practical applications, WPT systems with loosely coupled resonators are of interest due to the increased coupling transmission distance. We define the loosely coupled regime in terms of the normalized bandwidth as $\Delta < 0.2$. Within the loosely coupled regime, the inductance in the series topology is in the μH range, while the inductance in the shunt topology is in the nH range.

The difference in the inductances required for each topology impacts the potential WPT applications. In biomedical applications such as implantable medical devices, wearable electronics, and sensors, the transmitting and receiving coils should be small [41], which consequently results in short

transmission distances, and the shunt-shunt resonator topology may be a preferred choice. Conversely, for applications where large inductors are required for power transmission over mid-range distances, such as EV charging systems, smart home devices, and portable devices, the series-series topology may be the preferred choice. Therefore, a preliminary design study can be easily done using filter design concepts to evaluate inductor size in IPT links. The choice between the two topologies may also have an impact on the quality factor of the coils, with the series-series resonator topology potentially having larger quality factors due to the increased number of turns required for a larger inductor.

5. EXPERIMENTAL VERIFICATION

The four design examples described in Section 3 were built and tested. The primary objective of the experimental measurements was to verify and support the theory presented in the paper. All the coils were implemented in a planar spiral geometry fabricated on a 1.57 mm thick FR4 substrate with a copper thickness of 35 µm (1 oz copper).

The coil geometry is shown in Fig. 7(a). The number of turns n, inner diameter d, trace width w, and turn-to-turn spacing S determine the self-inductance of the structure, while the distance between coils determines the mutual inductance. A multi-coil IPT link with spiral inductors is shown in Fig. 7(c). The spacing between adjacent coils is defined as $\ell_{(j-1)(j)}$ where $j = 2, 3, 4, \ldots, N$.

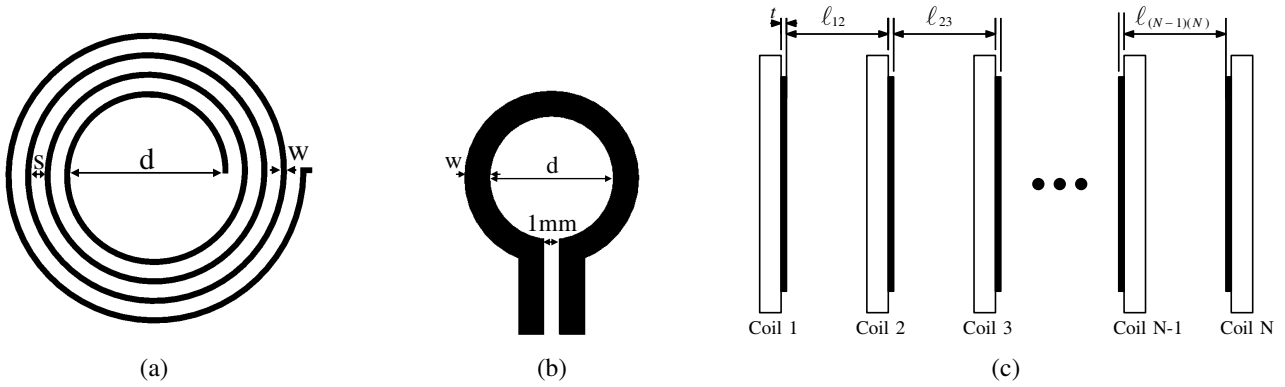

Figure 7. The geometry of a spiral inductor is shown in (a). The inductor is defined by an inner diameter d with n turns that have a turn-to-turn spacing S and trace width w. Inductors with one turn are built with a single circular loop shown in (b). A multi-coil IPT link is shown in (c). The coil spacing is defined as $\ell_{(j-1)(j)}$ where $j = 2, 3, 4, \ldots, N$.

The physical parameters for each inductor were first estimated using well-known equations found in [42]. We then used the full-wave finite-element-method (FEM) solver in COMSOL Multiphysics to finalize the geometric parameters of each inductor and characterize the mutual inductance between the two inductors with respect to separation distance. The full-wave simulator also modeled interwinding capacitance that needs to be included in the calculation of corresponding resonator capacitances.

The series-series second-order IPT link requires resonator inductances of 2.59 µH and series matching capacitances of 13.4 pF. The critical coupling transmission distance for the link is 7.2 cm. With reference to Fig. 7(a), the inductors have 2.5 mm wide (w) traces, four turns (n), an inner diameter (d) of 62.7 mm, and a trace spacing (S) of 6 mm. An additional copper trace and a chip capacitor are added to the back of the board to implement the complete resonator. The back side trace is connected to the top side inductor through a via. A photo of the experimental prototype is shown in Fig. 8(a).

The IPT links with shunt-shunt resonator coupling have nH-level inductors that are implemented with single turns ($n = 1$), as shown in Fig. 7(b). The diameter of the loop d is adjusted for the required inductance. Trace extensions are added to the loop to add matching capacitors on the board. The gap between the extension traces is 1 mm for all single-turn inductors described in this section.

The shunt-shunt second-order IPT link has resonators that require 22.80 nH inductors with shunt capacitances of 692.0 nF. The inductors were implemented using a 1.21 cm diameter loop. The critical

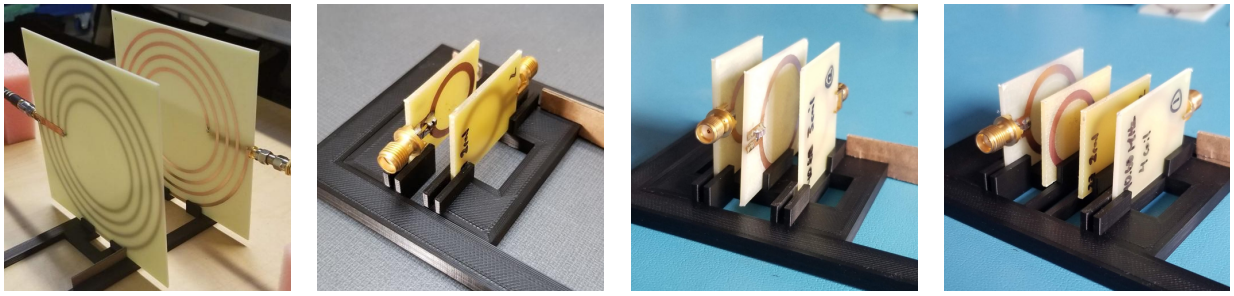

(a) (b) (c) (d)

Figure 8. Photographs of the experimental IPT systems. The second-order link in (a) has series-series resonator coupling and operates at 27.12 MHz. The IPT links in (b), (c), and (d) have shunt-shunt resonator coupling consist of two, three and four resonators respectively.

coupling distance for the IPT link is 0.8 cm, and this distance is used as a benchmark for the third and fourth order designs which couple power over larger distances. A photograph of the experimental prototype is shown in Fig. 8(b).

In the third-order shunt-shunt IPT link, the transmitter and receiver coils have an inductance of 32.20 nH, while the repeater coil is larger and has an inductance of 64.40 nH. The matching capacitors for the transmitter, repeater, and receiving resonators are 489.0 pF, 250.8 pF, and 489.0 pF, respectively. The repeater coil has a diameter of 2.90 cm, which is larger than the diameter of the transmitter and receiver coils. The overall transmission distance between the transmitter and receiver is approximately 1.60 cm. A photograph of the experimental prototype is shown in Fig. 8(c).

The fourth-order shunt-shunt IPT link has four resonators: the transmitter, receiver, and two repeaters. The transmitter and receiver resonators have the same size, and each resonator has an inductance of 42.34 nH shunted by a capacitance of 374.0 pF. The scaling factors for the repeater resonators are $m_{21} = m_{31} = 0.4$ which corresponds to an 0.8 cm gap between adjacent resonators under critical coupling conditions. As a consequence, the repeater coils have a smaller inductance and size than the coils in the transmitter and receiver. A photograph of the experimental prototype is shown in Fig. 8(d).

The frequency response (S_{21}) of the IPT links was measured with a PNA-X vector network analyzer from Keysight Technologies. The measured frequency response for each IPT design is shown in Figs. 9(a), (b), (c), and (d). The figures also include simulation results for comparison. For the third- and forth-order IPT links an additional simulation result including cross-coupling is included for reference so that the effect of cross-coupling, which was neglected in the analysis, can be evaluated. The cross coupling terms were extracted from our full-wave simulation in COMSOL Multiphysics.

Due to the large self-capacitance of the 2.56 µH-inductor in the second-order IPT link with series-series resonator coupling, the matching capacitance was modified from 13.3 pF to 10.7 pF to center the frequency response at 27.12 MHz. The most pronounced discrepancy between the measured and simulated results in Figs. 9(a) and Fig. 9(b) is the insertion loss of the filters. The minimum insertion loss is approximately 0.67 dB and 0.77 dB for the links with series-series and shunt-shunt resonator coupling, respectively. The insertion loss is attributed to the inductor quality factor where the Q of $L_{1,\mathrm{S}}$ in the series-series case is 115, while the Q of $L'_{1,\mathrm{P}}$ in the shunt-shunt case is 110. The shunt-shunt case has a lower inductance quality factor, and consequently insertion loss is expected to be higher in the shunt-shunt case. Using Equation (22), the analytic estimates of loss from finite Q are 0.67 dB for the series-series resonator link and 0.70 dB for the shunt-shunt resonator link.

The results for the third-order shunt-shunt IPT link are shown in Fig. 9(c). Two simulated results are shown to evaluate the effect of cross-coupling terms in the model. The cross-coupling does not have a significant effect on the frequency response of the link because the repeater coil (middle resonator) is larger than the input and output coils. The experimental results for the third-order IPT are also shown in the figure. The insertion loss at a frequency or 40.68 MHz is 0.87 dB. Note that with the addition of a repeater coil in the third-order link, the transmission distance is increased to 1.6 cm from 0.8 cm in the

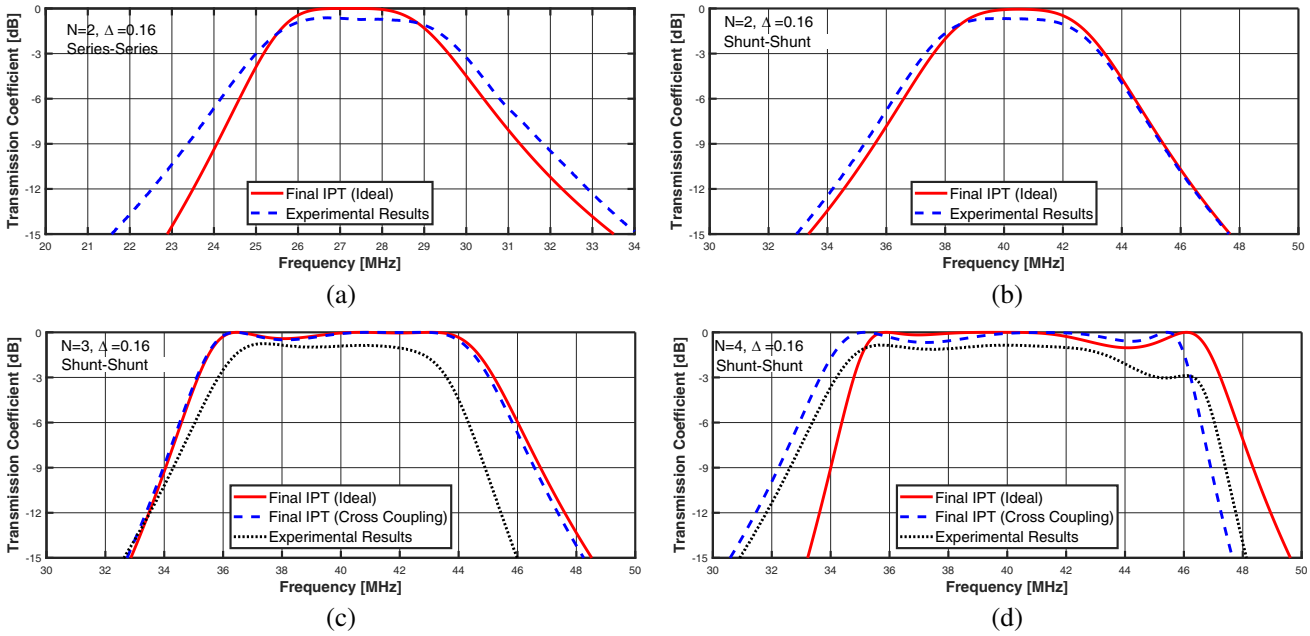

Figure 9. Simulated and measured transmission responses for different IPT links. The simulated response of the final transformed network is labelled as "Final IPT". Simulation responses are also provided including cross-coupling in third and fourth order designs. (a) is the frequency response of the second-order link with series-series coupled resonators. (b), (c), and (d) are associated with shunt-shunt transmission links with second-, third-, and fourth-order. The impedance scaling factor k_z and relative frequency bandwidth are 50 and 0.16, respectively, for all designs.

second-order system. The repeater coil in the third-order link increases the center frequency insertion loss by 0.10 dB relative to a two coil system.

Results for the fourth order shunt-shunt IPT link are shown in Fig. 9(d). A comparison of simulation results with and without cross-coupling shows that cross-coupling leads to a shift in the frequency response and an additional dip in the passband. The impact of cross-coupling on the performance of the fourth-order system is higher than the third-order link and relates to the smaller size ratio of the repeater coils with respect to the coils in the transmitter and receiver. The fourth-order link has a minimum insertion loss of 0.89 dB at 40.68 MHz, which is comparable to the insertion loss of the third-order link, while achieving a longer overall transmission distance of 2.4 cm. A summary of all the measurements is provided in Table 6.

Table 6. A summary of IPT measurements is provided.

Order (N)	Topology	Frequency (MHz)	Loss (dB)	Efficiency (%)	Bandwidth (%)
2	series-series	27.12	0.67	85.7	18.2
2	shunt-shunt	40.68	0.70	85.2	14.6
3	shunt-shunt	40.68	0.87	81.8	19.2
4	shunt-shunt	40.68	0.89	81.5	26.9

6. CONCLUSION

The application of canonical filter theory for synthesizing IPT systems was expanded to include networks with shunt-shunt coupling topologies with an arbitrary number of resonators. For the shunt-shunt topology there were additional approximations that were needed to convert the filter network into a realizable IPT network consisting of inductively coupled resonators. The L-matching network in the repeater resonators was replaced with a capacitor with the impedance level of the system held constant at the center frequency. Exact design equations were given for IPT systems with shunt-shunt coupling up to five resonators. Simplified expressions for the IPT network were also derived by neglecting higher order terms with Δ^2. The equations provide a systematic and elegant way to synthesize an initial IPT design that can be subsequently optimized using more complex field solvers that include the physical design of the coils.

The canonical filter design methodology also provides a systematic way to conduct comparative studies of different parameters that are relevant to IPT system implementation. An example was given by comparing the relative size of inductors that would be required to implement series-series matching at the terminal ports versus shunt-shunt matching at the terminal ports. The shunt-shunt topology leads to significantly smaller inductors for the same impedance, frequency, and bandwidth conditions. Small inductor size has benefits in sensor applications, while larger inductors have the advantage of increased power transfer distances. Therefore, there may be specific topologies that are more beneficial to a particular application. The wealth of knowledge from filter theory, which includes many different canonical forms, can be exploited by applying circuit transformations to realize coupled resonators that can be physically realized to implement IPT systems. The application of the filter design methodology was demonstrated by implementing four different IPT links which includes configurations that had a transmitter, receiver, and one or two repeater coils.

REFERENCES

1. Peek, G. A., M. R. Francis, and T. W. Frank, "Wireless charging device for wearable electronic device," US Patent 9,843,214, Dec. 12, 2017.
2. RamRakhyani, A. K., S. Mirabbasi, and M. Chiao, "Design and optimization of resonancebased efficient wireless power delivery systems for biomedical implants," *IEEE Transactions on Biomedical Circuits and Systems*, Vol. 5, No. 1, 48–63, 2010.
3. Ebrahimzadeh, E., M. Asgarinejad, S. Saliminia, S. Ashoori, and M. Seraji, "Predicting clinical response to transcranial magnetic stimulation in major depression using time-frequency EEG signal processing," *Biomedical Engineering: Applications, Basis and Communications*, Vol. 33, No. 6, 2150048, 2021.
4. Xie, L., Y. Shi, Y. T. Hou, and H. D. Sherali, "Making sensor networks immortal: An energy-renewal approach with wireless power transfer," *IEEE/ACM Transactions on Networking*, Vol. 20, No. 6, 1748–1761, 2012.
5. Hasan, N., I. Cocar, T. Amely, H. Wang, R. Zane, Z. Pantic, and C. Bodine, "A practical implementation of wireless power transfer systems for socially interactive robots," *2015 IEEE Energy Conversion Congress and Exposition (ECCE)*, 4935–4942, IEEE, 2015.
6. Miller, J. M., P. H. Chambon, P. T. Jones, and C. P. White, "Wireless power transfer electric vehicle supply equipment installation and validation tool," US Patent A13/544,058, Jan. 24, 2013.
7. Ahmad, A., M. S. Alam, and R. Chabaan, "A comprehensive review of wireless charging technologies for electric vehicles," *IEEE Transactions on Transportation Electrification*, Vol. 4, No. 1, 38–63, 2018.
8. Sinha, S., A. Kumar, B. Regensburger, and K. K. Afridi, "A new design approach to mitigating the effect of parasitics in capacitive wireless power transfer systems for electric vehicle charging," *IEEE Transactions on Transportation Electrification*, Vol. 5, No. 4, 1040–1059, 2019.
9. Kiani, M. and M. Ghovanloo, "The circuit theory behind coupled-mode magnetic resonance-based wireless power transmission," *IEEE Transactions on Circuits and Systems I: Regular Papers*, Vol. 59, No. 9, 2065–2074, Sep. 2012.

10. Zhang, W. and C. C. Mi, "Compensation topologies of high-power wireless power transfer systems," *IEEE Transactions on Vehicular Technology*, Vol. 65, No. 6, 4768–4778, 2015.
11. Thackston, K. A., H. Mei, and P. P. Irazoqui, "Coupling matrix synthesis and impedance-matching optimization method for magnetic resonance coupling systems," *IEEE Transactions on Microwave Theory and Techniques*, Vol. 66, No. 3, 1536–1542, 2017.
12. Yi, L. and J. Moon, "Design of efficient double-sided LC matching networks for capacitive wireless power transfer system," *2021 IEEE PELS Workshop on Emerging Technologies: Wireless Power Transfer (WoW)*, 1–5, IEEE, 2021.
13. Chen, Y., M. Li, B. Yang, S. Chen, Q. Li, Z. He, and R. Mai, "Variable-parameter T-circuit-based IPT system charging battery with constant current or constant voltage output," *IEEE Transactions on Power Electronics*, Vol. 35, No. 2, 1672–1684, 2019.
14. Huang, L., A. P. Hu, A. K. Swain, and Y. Su, "Z-impedance compensation for wireless power transfer based on electric field," *IEEE Transactions on Power Electronics*, Vol. 31, No. 11, 7556–7563, 2016.
15. Sinha, S., A. Kumar, S. Pervaiz, B. Regensburger, and K. K. Afridi, "Design of efficient matching networks for capacitive wireless power transfer systems," *2016 IEEE 17th Workshop on Control and Modeling for Power Electronics (COMPEL)*, 1–7, IEEE, 2016.
16. Keeling, N., G. A. Covic, F. Hao, L. George, and J. T. Boys, "Variable tuning in LCL compensated contactless power transfer pickups," *2009 IEEE Energy Conversion Congress and Exposition*, 1826–1832, IEEE, 2009.
17. Regensburger, B., A. Kumar, S. Sinha, K. Doubleday, S. Pervaiz, Z. Popovic, and K. K. Afridi, "High-performance large air-gap capacitive wireless power transfer system for electric vehicle charging," *2017 IEEE Transportation Electrification Conference and Expo (ITEC)*, 638–643, IEEE, 2017.
18. Regensburger, B., J. Estrada, A. Kumar, S. Sinha, Z. Popovic, and K. K. Afridi, "High-performance capacitive wireless power transfer system for electric vehicle charging with enhanced coupling plate design," *2018 IEEE Energy Conversion Congress and Exposition (ECCE)*, 2472–2477, IEEE, 2018.
19. Monti, G., A. Costanzo, F. Mastri, and M. Mongiardo, "Optimal design of a wireless power transfer link using parallel and series resonators," *Wireless Power Transfer*, Vol. 3, No. 2, 105–116, 2016.
20. Lee, J., Y.-S. Lim, W.-J. Yang, and S.-O. Lim, "Wireless power transfer system adaptive to change in coil separation," *IEEE Transactions on Antennas and Propagation*, Vol. 62, No. 2, 889–897, 2013.
21. Lee, J., Y. Lim, H. Ahn, J.-D. Yu, and S.-O. Lim, "Impedance-matched wireless power transfer systems using an arbitrary number of coils with flexible coil positioning," *IEEE Antennas and Wireless Propagation Letters*, Vol. 13, 1207–1210, 2014.
22. Barakat, A., K. Yoshitomi, and R. K. Pokharel, "Design approach for efficient wireless power transfer systems during lateral misalignment," *IEEE Transactions on Microwave Theory and Techniques*, Vol. 66, No. 9, 4170–4177, 2018.
23. Ahmadi, M., T. VanderMeulen, L. Markley, and T. Johnson, "Adaptive load impedance compensation theory for inductive power transfer systems," *2022 IEEE Wireless Power Transfer Conference (WPTC)*, 1–6, 2022.
24. Awai, I. and T. Ishizaki, "Design of 'magnetic resonance type' WPT systems based on filter theory," *Electronics and Communications in Japan*, Vol. 96, No. 10, 1–11, 2013.
25. Awai, I. and T. Komori, "A simple and versatile design method of resonator-coupled wireless power transfer system," *2010 International Conference on Communications, Circuits and Systems (ICCCAS)*, 616–620, 2010.
26. Awai, I. and T. Ishizaki, "Superiority of BPF theory for design of coupled resonator WPT systems," *Asia-Pacific Microwave Conference 2011*, 1889–1892, IEEE, 2011.
27. Peng, C., Z. Chen, Z. Xu, Z. Zhao, J. Li, and H. Zhao, "A systematic design method for a wireless power transfer system based on filter theory," *IEEE Transactions on Microwave Theory and Techniques*, Vol. 70, No. 4, 2407–2417, 2022.

28. Awai, I., "Design theory of wireless power transfer system based on magnetically coupled resonators," *2010 IEEE International Conference on Wireless Information Technology and Systems*, 1–4, IEEE, 2010.
29. Zhang, J. and C. Cheng, "Comparative studies between KVL and BPFT in magnetically-coupled resonant wireless power transfer," *IET Power Electronics*, Vol. 9, No. 10, 2121–2129, 2016.
30. Ahmadi, M., L. Markley, and T. Johnson, "A filter theory approach to the synthesis of capacitive power transfer systems," *IEEE Journal of Emerging and Selected Topics in Power Electronics*, Vol. 10, No. 1, 91–103, 2020.
31. VanderMeulen, T., M. Ahmadi, L. Markley, and T. Johnson, "Comparison of shunt-shunt and series-series resonator topology for second-order WPT systems," *2022 Wireless Power Transfer Conference (WPTC)*, 1–4, 2022.
32. Awai, I., T. Komori, and T. Ishizaki, "Design and experiment of multi-stage resonator-coupled WPT system," *2011 IEEE MTT-S International Microwave Workshop Series on Innovative Wireless Power Transmission: Technologies, Systems, and Applications*, 123–126, 2011.
33. Luo, B., S. Wu, and N. Zhou, "Flexible design method for multi-repeater wireless power transfer system based on coupled resonator bandpass filter model," *IEEE Transactions on Circuits and Systems I: Regular Papers*, Vol. 61, No. 11, 3288–3297, 2014.
34. Matthaei, G., L. Young, and E. Jones, "Design of microwave filters, impedance-matching networks, and coupling structures: Volume 1," Tech. Rep., Stanford Research Institute, Menlo Park, CA, 1963.
35. Badowich, C., J. Rousseau, and L. Markley, "Convex optimization of coil spacing in cascaded multi-coil wireless power transfer," *Wireless Power Transfer*, Vol. 7, No. 1, 42–50, 2020.
36. Matthaei, G., "Properties of some common microwave filter elements," *Microwave Filters, Impedance-Matching Networks, and Coupling Structures*, Vol. 5, 149–155, 1980.
37. Zverev, A., *Handbook of Filter Synthesis*, 1st Edition, John Wiley & Sons, New York, 1967.
38. Hunter, I., "Theory and design of microwave filters," *IET*, No. 48, 125–136, 2001.
39. Cohn, S. B., "Dissipation loss in multiple-coupled-resonator filters," *Proceedings of the IRE*, Vol. 47, No. 8, 1342–1348, 1959.
40. Cadence, I., *Design Systems, AWR Microwave Office Getting Started Guide*, San Jose, California, USA, 2022.
41. Khan, S. R. and G. Choi, "Analysis and optimization of four-coil planar magnetically coupled printed spiral resonators," *Sensors*, Vol. 16, No. 8, 1219, 2016.
42. Terman, F. E., *Radio Engineers' Handbook*, McGRAW-HILL Book Company, INC., New York and London, 1943.